Supporting Information

In Situ Nanoscale Investigation of Catalytic Reactions in the Liquid Phase using Zirconia-protected Tip-enhanced Raman Spectroscopy Probes

Naresh Kumar[†‡§], Caterina S. Wondergem[†§] Andrew J. Wain[‡] and Bert M. Weckhuysen[†*]

[†] Faculty of Science, Debye Institute for Nanomaterials Science, Utrecht University, Universiteitsweg 99, Utrecht 3584 CG, The Netherlands
[‡] National Physical Laboratory, Hampton Road, Teddington, Middlesex, United Kingdom TW11 0LW
[§]These authors contributed equally to this work
*Email: B.M.Weckhuysen@uu.nl

S1. Experimental details

S.1.1 TERS system

A bespoke transmission-mode TERS system was used in this work consisting of an AFM (AIST-NT, USA) positioned on top of an inverted confocal Raman microscope (Nikon, Japan), which was attached to a Raman spectrometer (HORIBA Scientific, France) fitted with a charged coupled device detector (Andor, Ireland). All far-field and TERS measurements were performed using a radially-polarized 532 nm excitation laser that was focused on the sample using a 100x, 1.49 NA, oil immersion objective lens (Nikon, Japan). In the confocal Raman microscope, the diameter of the excitation laser spot at the sample was estimated from the far-field spatial resolution measured using a line Raman map across a SWCNT to be ≈ 450 nm. TERS measurements were carried out using contact-mode AFM feedback. A laser power of 50 - 117 μW at the sample was used for the far-field and TERS measurements. For performing TERS measurements, the TERS probe was first aligned with the excitation laser. Then, the sample was moved in a raster fashion between the TERS probe and objective lens, whilst a TERS spectrum was measured at each pixel. Mapping of pATP → DMAB at the TERS probe-apex was performed by first aligning the TERS probe with the laser-spot. Then, the objective lens was moved in a raster fashion around the TERS probe whilst keeping the sample and the probe stationary and measuring a Raman spectrum at each pixel. All TERS spectra presented in this work comprise sum of Raman signals generated in the near-field as well as far-field. Data analysis was performed using OriginPro, SPIP™, AIST-NT SPM, MATLAB and LabSpec 5 software. All TERS, SERS and far-field Raman spectra were smoothed and vertically shifted for easier visualization of vibrational bands.

S.1.2 Sample preparation

The PEDOT:PSS thin film sample was prepared by spin-coating an aqueous solution of PEDOT:PSS (Heraeus Precious Metals GmbH & Co., Germany) onto a glass coverslip (thickness number: 1.5) at 2000 revolutions per min for 2 min under argon atmosphere. The Ag substrate was prepared by thermal deposition of 10 nm Ag (Advent Research Materials, UK, 99.99%) on a glass coverslip at 10^{-6} mbar pressure. The pATP (Sigma Aldrich, UK, 97%) SAM was prepared by immersing the Ag substrate in 10 mM pATP solution in ethanol (Fisher Scientific, UK, 99.99%) for 2 h. The pATP-functionalized Ag substrate was

subsequently rinsed with copious amount of ethanol and deionized water to remove any surface residuals.

S.1.3 Transmission electron microscopy (TEM) characterization

TEM measurements were performed on a Talos F200X (FEI) electron microscope operating at 200 keV. Each TERS probe was mounted on a high tilt holder and its apex was measured under 71° angle. TEM images were analyzed using iTEM 5.0 software.

S.1.4 Preparation of TERS probes

TERS probes were prepared in two stages as follows:

S.1.4.1 Multi-layer metal coating

First, a multilayer coating of 3 nm Cr, 10 nm Au and 100 nm Ag was deposited on commercial AFM probes (MikroMasch, USA) using thermal evaporation at a pressure of 10^{-6} mbar. The average apex-diameter of the TERS probes was estimated from the scanning electron microscopy (SEM) measurements to be ≈ 50 nm.

S.1.4.2 ZrO_2 coating

A thin layer of ZrO_2 was coated on top of the multi-layer metal-coated TERS probes using the following three step procedure. A schematic diagram of the coating procedure is presented in Figure S1:

Step 1. (3-aminopropyl)trimethoxysilane (APTMS) was adsorbed on the Ag surface of metal-coated TERS probes by immersing them in 8 μM solution of APTMS in MilliPore water (resistivity 18.2 MΩ cm) for 15 min at room temperature.

Step 2. Immersion of the APTMS-functionalized TERS probes in 2.5 mM zirconium (IV) propoxide solution in 1-propanol resulted in the condensation of the ZrO_2 precursor. APTMS serves as an anchor for ZrO_2 growth. In order to achieve a thin, uniform, pinhole-free coating, the solution was placed in a 3:1 ice:NaCl bath (-18°C) in order to slow down the reaction rate. The reaction temperature was found to be a critical factor affecting the growth of ZrO_2 layer. See Figure S2 for a comparison of ZrO_2 coatings performed at different temperatures on Au nanoparticles.

Step 3. The ZrO_2-protected probes were washed by dipping them alternately in 1-propanol, MilliPore water, 1-propanol, MilliPore water, ethanol, MilliPore water and ethanol.

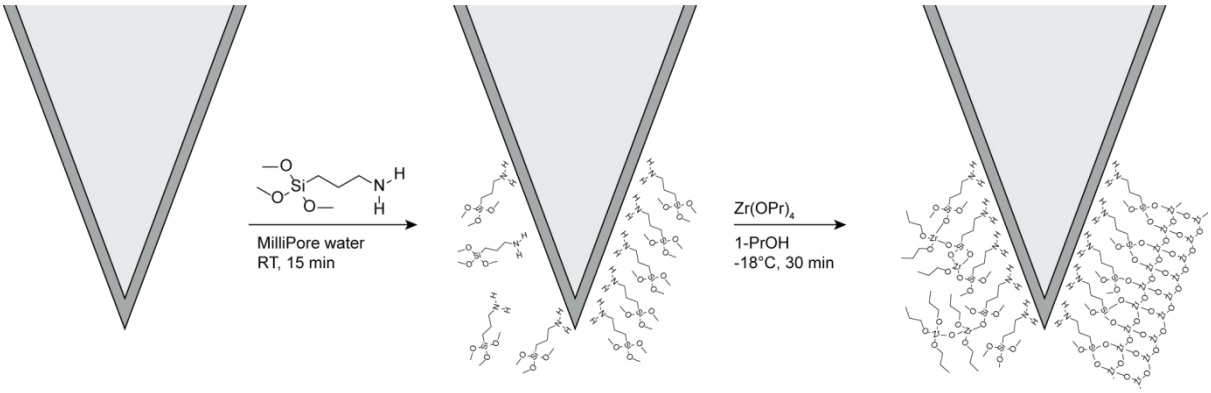

Figure S1. Schematic diagram illustrating the procedure for producing ultrathin ZrO_2 layer over Ag-coating of TERS probes.

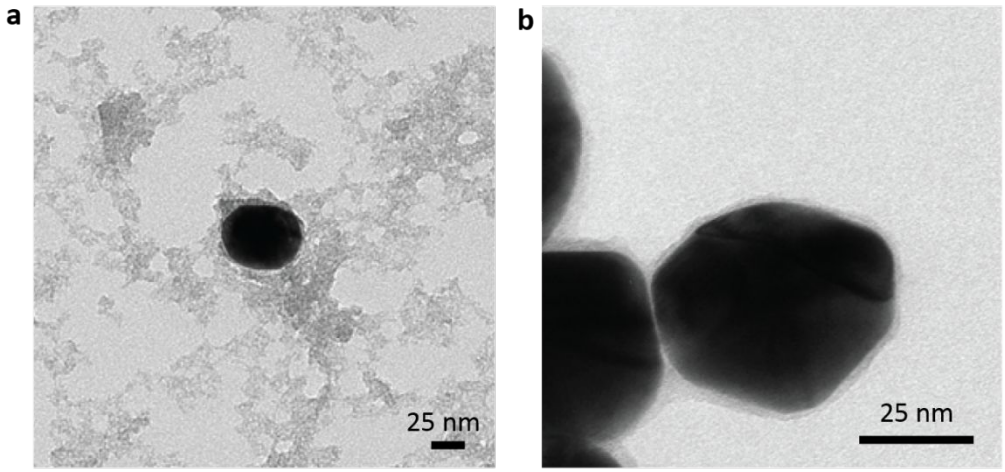

Figure S2. a) TEM image of a Au nanoparticle subjected to the ZrO_2 coating procedure at room temperature. A rapid reaction rate results in an uncontrolled nucleation and growth of ZrO_2 throughout the sample. **b)** TEM image of Au nanoparticles subjected to the ZrO_2 coating procedure at -18°C using 3:1 ice:NaCl bath. At -18°C, a slow reaction rate yields a smooth and pinhole-free ZrO_2 layer at the surface of Au nanoparticles.

We tested the stability of ZrO_2 coating in solutions of different pH as shown in Figure S3.

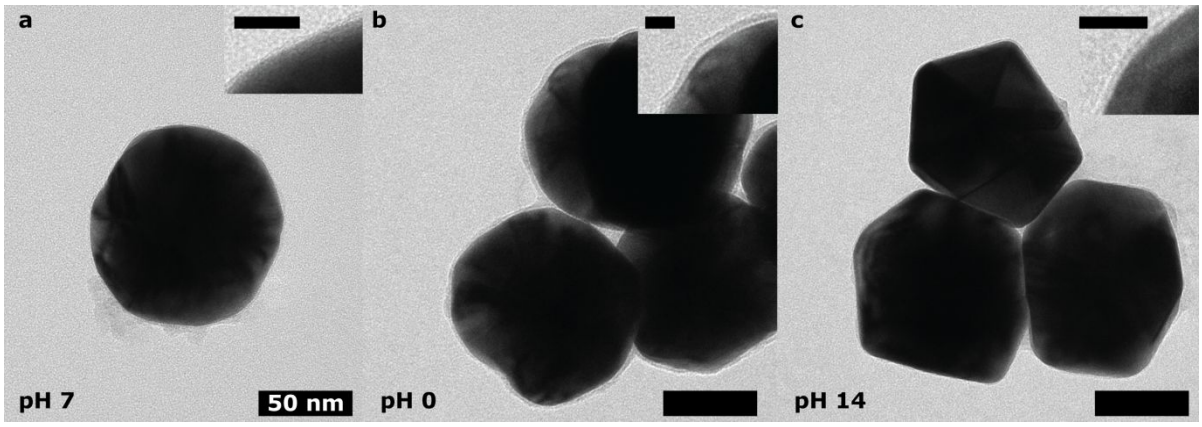

Figure S3. Au@ZrO_2 nanoparticles were prepared following the method described above. After the washing steps the NPs were redispersed in solutions with different pH for 30 – 45 minutes and subsequently the stability of the ZrO_2 layer was assessed using TEM. **a)** TEM

image of a reference Au@ZrO_2 nanoparticle dispersed in a solution of pH ≈7. **b)** TEM image of Au@ZrO_2 nanoparticles redispersed in a solution of pH 0 (1 M HCl in MilliPore water). **c)** TEM image of Au@ZrO_2 nanoparticles redispersed in a solution of pH 14 (1 M NaOH in MilliPore water). Scale bars: 50 nm; scale bars for insets: 10 nm. The Au nanoparticles are found to be fully covered with a ZrO_2 layer after exposure to both pH 0 and pH 14 environments, demonstrating the high stability of the ZrO_2 coating.

We also tested the stability of ZrO_2 coating in an aqueous environment over a long period of time as shown in Figure S4.

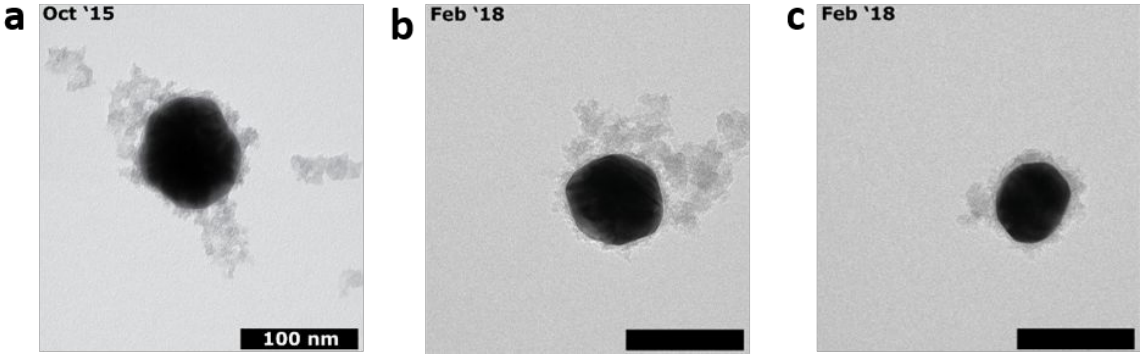

Figure S4. Au@ZrO_2 nanoparticles prepared following the unoptimized method described in Figure S2a. Instead of carrying out the coating at -18°C, room temperature was used, resulting in uncontrolled ZrO_2 growth. **a)** TEM image of unoptimized Au@ZrO_2 nanoparticles after synthesis in October 2015. **b), c)** TEM images of the same unoptimized Au@ZrO_2 nanoparticle sample after storage in water at room temperature for 2 years and 5 months. All scale bars: 100 nm. No significant change in the ZrO_2 coating was observed, demonstrating high stability in a liquid environment over time.

Finally, we tested the stability of ZrO_2 coating on Ag coated TERS probes after TERS measurements in an aqueous environment as shown in Figure S5.

a

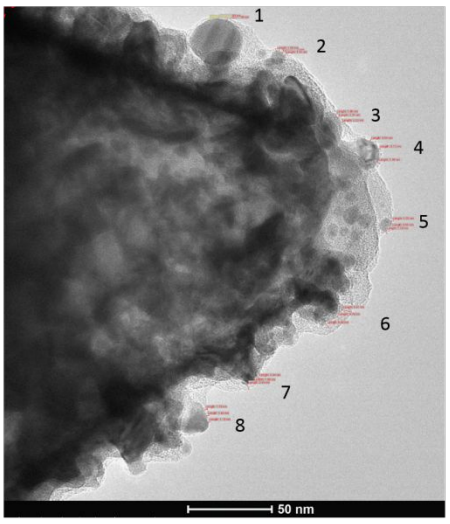

b

Location of zirconia coating	Thickness (nm)
1	1.4 ± 0.2
2	1.5 ± 0.2
3	2.2 ± 0.1
4	1.0 ± 0.3
5	1.2 ± 0.4
6	5.3 ± 0.4
7	1.8 ± 0.7
8	1.4 ± 0.2

c

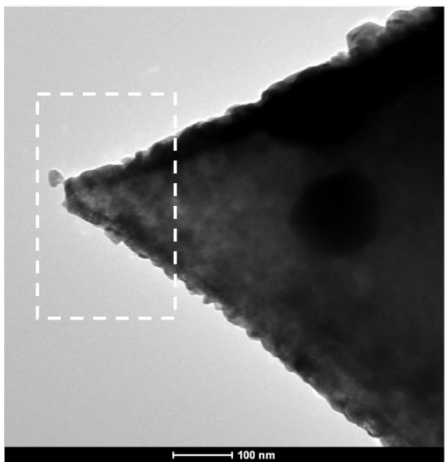

d

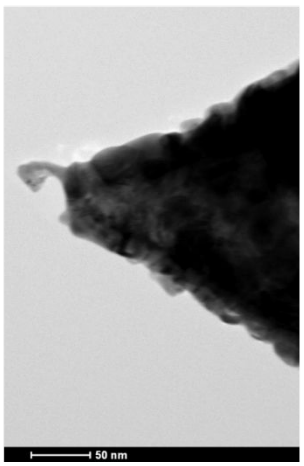

e

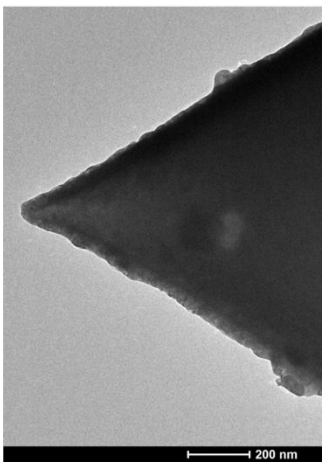

Figure S5. a) TEM image of a ZrO_2-protected TERS probe-apex after being used for continuous TERS measurements in water for ≈ 2 h. **b)** Average thickness of ZrO_2 coating measured using iTEM 5.0 software at the locations marked as 1 - 8 in Figure S5a. Individual measurement locations and thicknesses are marked in red in Fig. S5a. The thickness of the ZrO_2 layer on the Ag varies from 1 - 5 nm. This demonstrates the robustness and structural stability of ZrO_2 coating for TERS measurements within a liquid environment. The morphology of the ZrO_2 at the TERS probe-apex is uneven because of the grainy nature of the underlying Ag coating. Ag deposition using thermal evaporation in a vacuum chamber typically produces a rough metallic layer containing nanoscale size grains (*Phys. Chem. Chem. Phys.,* 2016, **18**, 13710-13716), which are essential for the excitation of a strong LSPR at the TERS probe-apex (*Chem. Soc. Rev.*, 2017,**46**, 3922-3944). **c)** TEM image of a Ag-coated TERS tip without ZrO_2 protection. **d)** Zoomed-in TEM image of the area highlighted in **c**. **e)** TEM image of a second Ag-coated tip without ZrO_2 protection. A significantly different surface morphology is observed at the Ag-coated tip-apex without ZrO_2 protection. Whilst the ZrO_2-protected tip-apex in **a** shows the presence of discrete Ag nanoparticles, a relatively smooth Ag-coating is observed in **d** and **e**. This suggests that the ZrO_2-coating procedure leads to further roughening of the Ag-coated TERS tip-apex, which could help preserve its plasmonic signal enhancement.

S2. Additional Figures

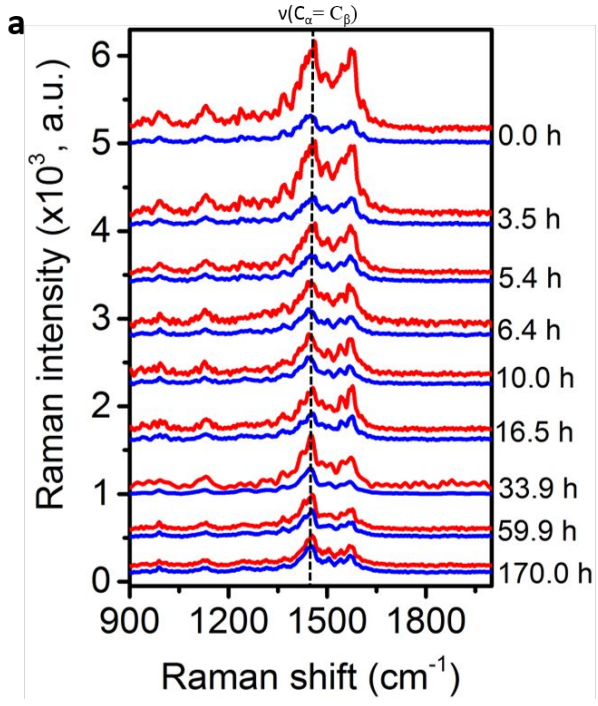

b

Exposure to ambient environment (Hours)	TERS contrast
0.0	2.9 ± 0.5
3.5	1.9 ± 0.1
5.4	1.1 ± 0.1
6.4	0.9 ± 0.1
10.0	0.7 ± 0.1
16.5	0.6 ± 0.1
33.9	0.5 ± 0.1
59.9	0.3 ± 0.1
170.0	0.1 ± 0.1

Figure S6. Plasmonic degradation of unprotected Ag-coated TERS probes in air. a) Time-series TERS (red) and far-field (blue) spectra measured using unprotected Ag-coated TERS probes on a PEDOT:PSS thin film after different durations (0 – 170 h) of exposure to the ambient environment. Integration time: 30 s. Laser power at the sample: 50 μW. **b)** Average TERS contrast 1454 cm^{-1} band intensity from three TERS and far-field measurements performed at the times shown in Figure S6a calculated using Eq. 1. Intensity of 1454 cm^{-1} band was determined from Lorentzian fitting of Raman bands in the 1313 -

1721 cm^{-1} range after linear background subtraction. TERS contrast decreases rapidly when unprotected TERS probes are exposed to the ambient environment indicating a fast degradation of their plasmonic sensitivity.

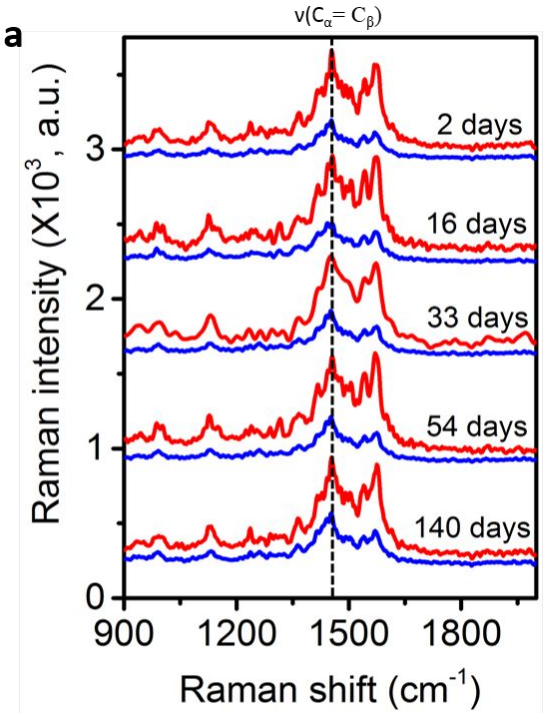

b

Exposure to the ambient environment (Days)	TERS contrast
2	1.36 ± 0.05
16	1.20 ± 0.04
33	1.14 ± 0.03
54	1.07 ± 0.02
140	0.77 ± 0.02

Figure S7. Extending lifetime of TERS probes using ZrO_2 protection. a) Time-series TERS (red) and far-field (blue) spectra measured using ZrO_2-protected TERS probes on a PEDOT:PSS thin film after different durations (2 – 140 days) of exposure to the ambient environment. Integration time: 30 s. Laser power at the sample: 50 µW. **b)** Average TERS contrast 1454 cm^{-1} band intensity from three TERS and far-field measurements performed at the times shown in Figure S7a calculated using Eq. 1. Intensity of 1454 cm^{-1} band was determined from Lorentzian fitting of Raman bands in the 1313 - 1721 cm^{-1} range after linear background subtraction. Due to the time required to transfer the ZrO_2-protected TERS probes across labs at the Utrecht University, Netherlands and the National Physical Laboratory, UK, TERS measurements of fresh ZrO_2 – protected probes ("0 days") couldn't be performed.

Contrast of the TERS probes decreases very gradually on exposure of the probes to the ambient environment indicating that the TERS probes do undergo some plasmonic degradation over time. However, the rate of degradation is significantly smaller compared to the unprotected Ag-coated TERS probes such that they still maintain some plasmonic activity after 4.5 months of exposure to the ambient environment.

Three different batches of ZrO_2 coated probes were used for the time-series TERS measurements: Batch 1: tested after 2 and 140 days, Batch 2: tested after 2 and 33 days,

Batch 3: tested after 16, 33 and 54 days. A similar plasmonic signal enhancement was observed in all three batches of the ZrO_2 coated TERS probes.

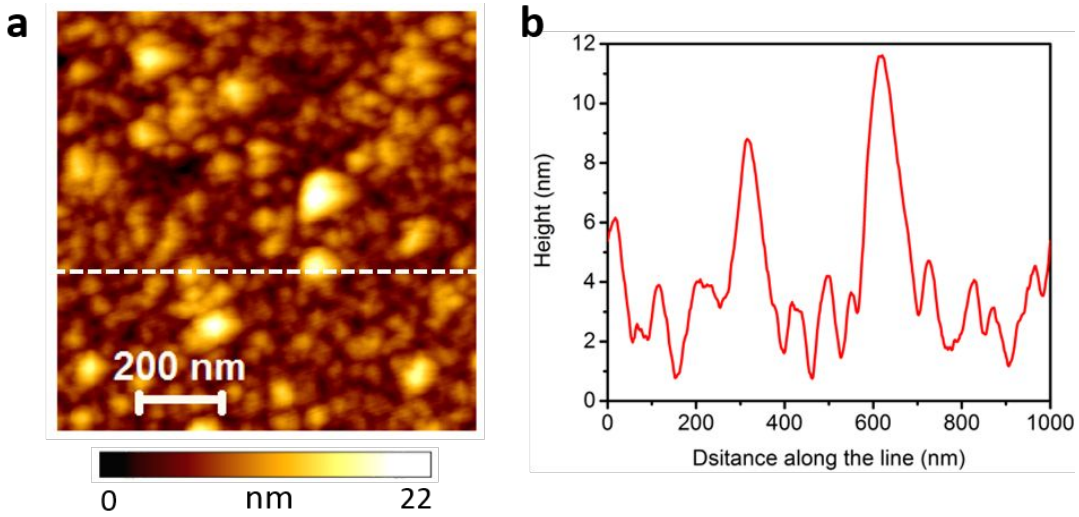

Figure S8. a) Tapping mode AFM topography image of pATP-functionalized Ag substrate used for mapping pATP → DMAB using TERS in this work. **b)** Height profile along the line marked in Figure S8a showing size variation of Ag nanostructures on the substrate. Along the line, the height of the Ag nanostructures on the heterogeneous Ag substrate varies from 1 – 9 nm.

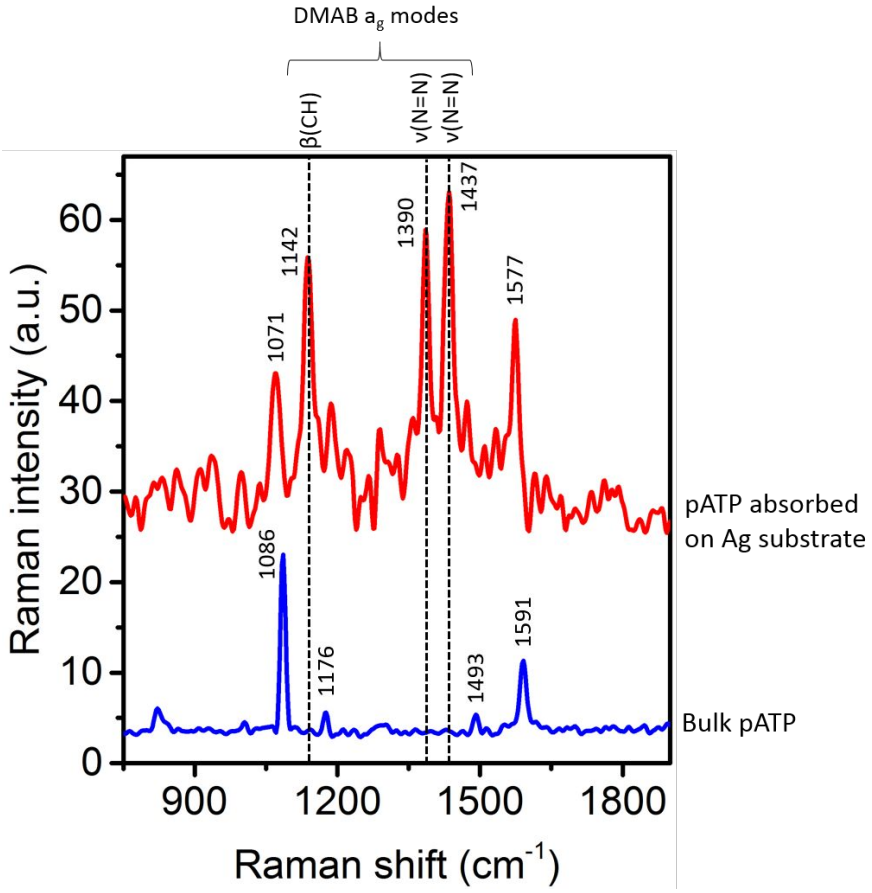

Figure S9. Comparison of Raman spectrum of bulk pATP and SERS spectrum of pATP adsorbed on heterogeneous Ag substrate. Confocal Raman spectrum (blue, integration time: 1 s) of bulk pATP (large aggregates placed on a glass substrate) and SERS spectrum of pATP (red, integration time: 60 s) adsorbed on a heterogeneous Ag substrate measured in air using a 532 nm excitation laser. Laser power at the sample: 117 µW. In the confocal Raman spectrum of bulk pATP, characteristic a_1 Raman bands of pATP are visible at 1086 cm^{-1}, 1176 cm^{-1}, 1493 cm^{-1} and 1591 cm^{-1}, whereas in the SERS spectrum of pATP adsorbed on a heterogeneous Ag substrate, characteristic Raman bands of DMAB are visible at 1071 cm^{-1}, 1142 cm^{-1}, 1390 cm^{-1}, 1437 cm^{-1} and 1577 cm^{-1}, indicating conversion of pATP → DMAB (*J. Am. Chem. Soc.,* 2010, **132**, 9244-9246).

On the SERS-active Ag substrate, DMAB is produced through dimerization of pATP at the sites where plasmonic Ag nanostructures exhibit strong LSPR with the excitation laser and within plasmonic SERS hotspots, the locations of strongest LSPR produced by gap-mode plasmons emerging between closely spaced plasmonic nanostructures. Therefore, the SERS spectrum represents the total amount of DMAB formed at all plasmonically active sites present within the probe area (≈1.6 × 10^5 nm^2) of the excitation laser spot at the sample surface.

Furthermore, 1086 cm^{-1} and 1591 cm^{-1} Raman bands of pATP overlap with the DMAB Raman bands at 1071 cm^{-1} (ν (C-S))and 1577 cm^{-1} (ν(C=C)), respectively. However, the pATP → DMAB reaction can be monitored using the DMAB a_g bands at 1142 cm^{-1} (β(C-H)), 1390 cm^{-1} (ν(N=N)), 1437 cm^{-1} (ν(N=N)), which appear at distinct spectral positions compared to the pATP Raman bands (*Phys. Chem. Chem. Phys.* 2012, **14**, 4095–4100, *Sci. Rep.* 2013, **3:2997**, 1-6, *ACS Catal.*, 2017, **7**, 7803-7809).

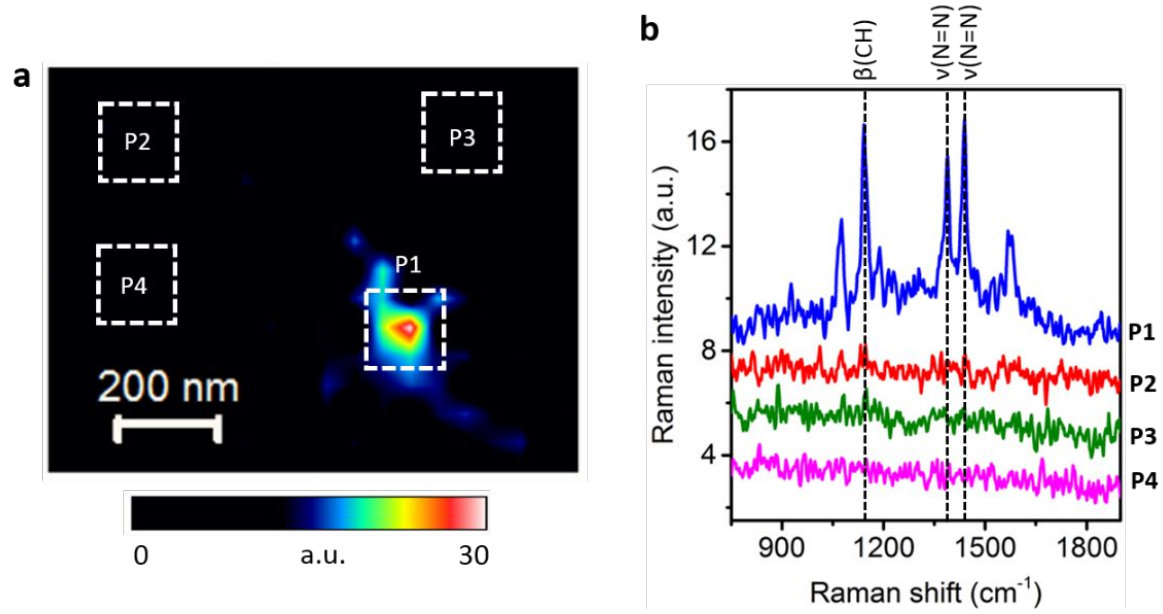

Figure S10. a) Map of pATP → DMAB at a TERS probe-apex obtained using the intensity of the 1437 cm^{-1} (ν(N=N)) DMAB Raman band measured from a pATP SAM on a Ag substrate in air. **b)** Average Raman spectra from 150 × 150 nm^2 areas at the probe-apex (P1) and away from the probe-apex (P2 – P4) marked in Figure S10a. Integration time: 1 s. Laser power at the sample: 117 μW. Note that the DMAB Raman bands are only visible in the average spectrum from location P1, indicating a strong LSPR at the TERS probe-apex enabling a sensitive detection of DMAB. Although no DMAB bands are visible in the average SERS spectra from locations P2 – P4 during the short integration time of 1 s, the DMAB bands do appear in the SERS spectrum when the integration time is increased to 60 s as shown in Figure S9.

Note that whilst the SERS spectrum (Figure S9) represents the DMAB molecules produced within the probe area of excitation laser spot (≈1.6 × 10^5 nm^2), the TERS spectrum (positon P1 in Figure S10a) results from the Raman signal of DMAB produced in a much smaller region at the probe-apex (≈7.1 × 10^2 nm^2) in addition to the SERS signal from the area around the probe.

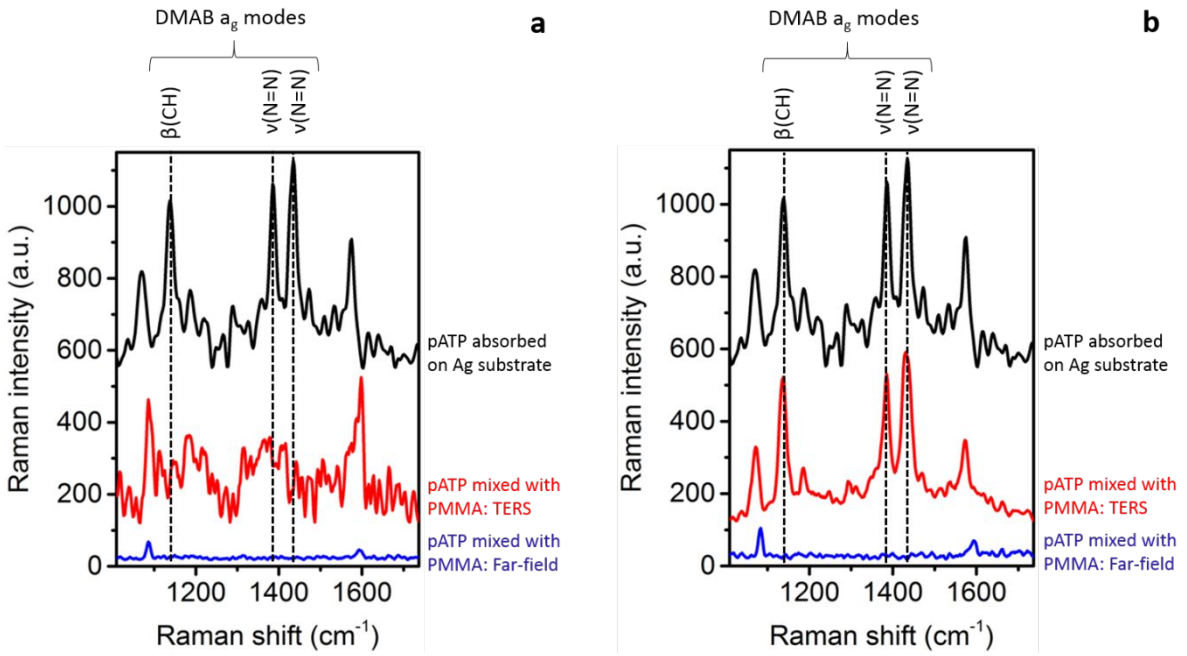

Figure S11. Chemical inertness test of ZrO_2-protected TERS probe. a) A ZrO_2-protected probe was placed in contact with a thin film of pATP mixed with PMMA spin-coated on a glass substrate and Raman mapping was carried out around the probe by moving the objective lens in a raster fashion. TERS spectrum measured at the TERS probe-apex and far-field spectrum measured with the TERS probe retracted from the sample are shown in red and blue respectively. Integration time: 60s. Laser power at the sample: 50 μW. SERS spectrum (black) of pATP adsorbed on a heterogeneous Ag substrate (from Figure S9) is also included for comparison. TERS spectrum shows absence of all DMAB a_g Raman bands. However, the a_1 Raman bands of pATP at 1086 cm^{-1} and 1591 cm^{-1} are enhanced by a contrast of 5.3 (measured using 1086 cm^{-1} band intensity) in the TERS near-field. **b)** Similar TERS measurements on a thin film of pATP mixed with PMMA spin-coated on a glass substrate with a Ag coated TERS probe without any ZrO_2 protection. In the TERS spectrum (red) measured at the probe-apex all DMAB a_g Raman bands are clearly visible confirming the pATP → DMAB reaction. Whereas, only pATP Raman band appear in the far-field spectrum (blue). Integration time: 60s. Laser power at the sample: 50 μW. These measurements demonstrate the chemical isolation of the Ag-coated probe afforded by the ZrO_2 protective layer.

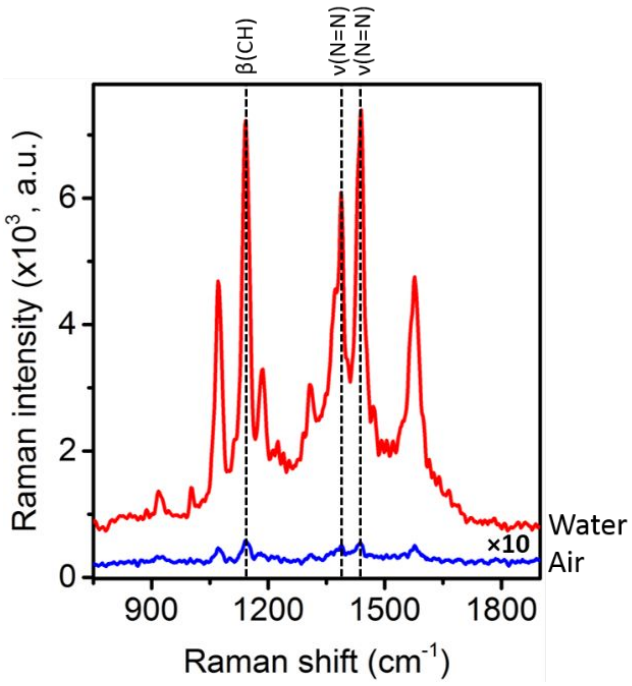

Figure S12. Comparison of pATP → DMAB SERS spectra measured in air and water environments. pATP → DMAB SERS spectra measured on a heterogeneous Ag substrate in air (blue) and water (red). Integration time: 60 s. Laser power at the sample: 117 μW. Note that the SERS spectrum in air has been multiplied by a factor of 10 for easier visualization. Interestingly, a 210× larger SERS signal (measured using the 1437 cm^{-1} DMAB band intensity) is observed in water compared to air. Similar observations were observed across three different samples. A higher SERS signal intensity in water possibly results from facile diffusion of pATP molecules into plasmonically active sites on the Ag substrate in water or redshift of the LSPR of the Ag SERS substrate, as discussed in the main text.

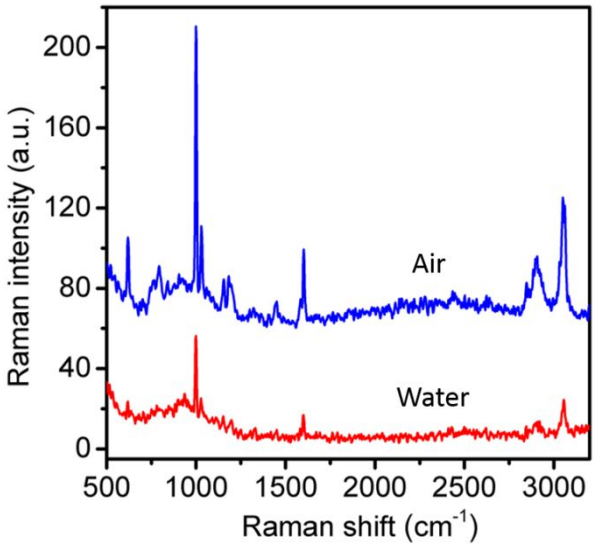

Figure S13. Far-field Raman spectra measured from a polystyrene thin-film on glass in air (blue) and water (red). Integration time: 60 s. Laser power at the sample: 170 µW. The Raman signal (measured using 1002 cm^{-1} band intensity) is reduced by a factor of 3.6× in water due to laser focus aberrations resulting in the loss of optical coupling.

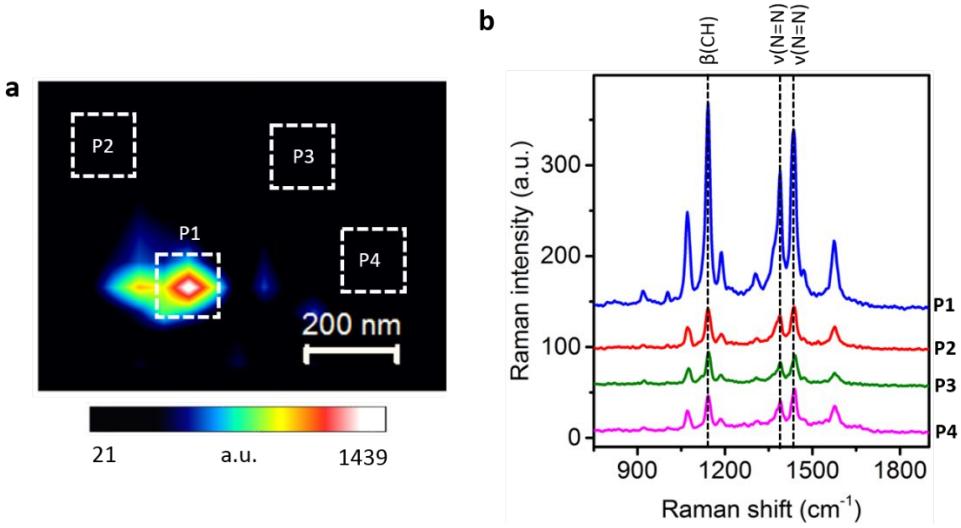

Figure S14. a) Map of pATP → DMAB at a TERS probe-apex obtained using the intensity of the 1437 cm^{-1} DMAB Raman band measured from pATP SAM on a Ag substrate in water. **b)** Average spectra from 150 × 150 nm^2 areas at the probe-apex (P1) and away from the probe-apex (P2 – P4) in Figure S14a. Integration time: 1 s. Laser power at the sample: 117 µW. A significantly enhanced intensity of DMAB Raman bands is observed in the average spectrum at P1 compared to other areas indicating a strong LSPR at the TERS probe-apex. Furthermore, spectra from all four locations in Figure S14a show a significantly higher signal to noise ratio compared to the corresponding measurements in air shown in Figure S10. Interestingly, average SERS spectra from areas away from the probe-apex (P2 – P4) in water show clear DMAB bands with an integration time of 1 s in contrast to the corresponding SERS spectra in air shown in Figure S10b where no DMAB bands are visible. This suggests facile diffusion of pATP molecules into plasmonically active sites on the heterogeneous Ag substrate within the aqueous environment or better overlap of the SERS substrate LSPR with the excitation laser wavelength as discussed in Figure S12.

Table S1. Calculation of the average intensity of DMAB bands (I_{DMAB}) to the intensity of 1071 cm^{-1} band (I_{1071}) ratio at locations P1 – P4 in Figure S14. I_{DMAB} is calculated from the average intensity of DMAB Raman bands at 1142 cm^{-1} (I_{1142}), 1390 cm^{-1} (I_{1390}) and 1437 cm^{-1} (I_{1437}). For comparison, I_{DMAB}/I_{1071} has also been calculated for the highest intensity spectrum observed in area P1 at the probe-apex. A similar I_{DMAB}/I_{1071} at the locations P1-P4 indicates that the ZrO_2-protected TERS probe does not interfere with the pATP → DMAB reaction but rather measures the extent of conversion at the sample surface. This further confirms the chemical inertness of the TERS probe rendered by ZrO_2 protection.

Location	I_{1071} (a.u.)	I_{1142} (a.u.)	I_{1390} (a.u.)	I_{1437} (a.u.)	$(I_{1142} + I_{1390} + I_{1437})/3$ (I_{DMAB})	I_{DMAB}/I_{1071}
P1	97	217	144	191	184	1.9
P2	22	43	35	46	41	1.9
P3	16	35	25	32	31	1.9
P4	21	38	33	46	39	1.9
Highest intensity spectrum in P1	197	428	244	361	344	1.8

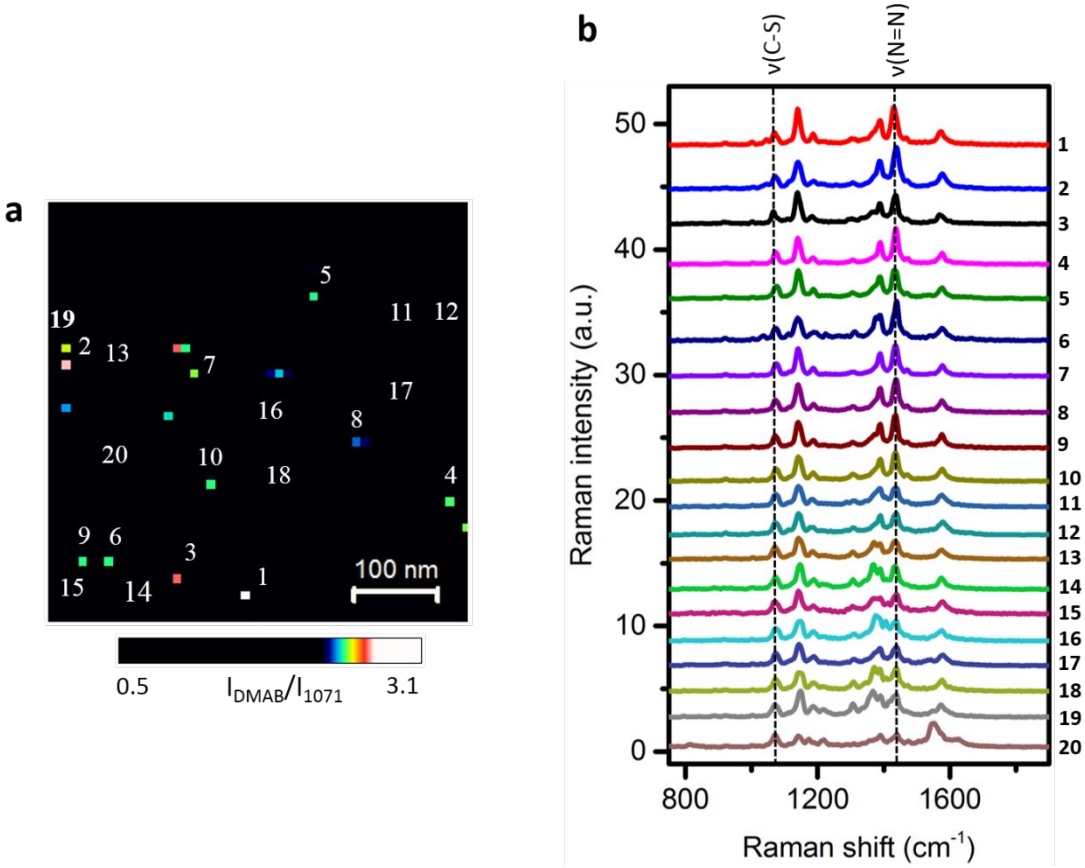

Figure S15. a) TERS map of pATP → DMAB conversion within an aqueous environment shown in Figure 4d with adjusted contrast to highlight regions of notably high activity. **b)** Plot of TERS spectra from ten different locations of high (marked 1 – 10 in Figure S15a) and low (marked as 11 – 20 in Figure S15a) I_{DMAB}/I_{1071} ratio. Spectra have been normalized to the intensity of Raman band at 1071 cm^{-1} for easier comparison. A higher I_{1437}/I_{1071} ratio is observed in the TERS spectra from positions 1 – 10 compared to 11 – 20 indicating that a greater amount of DMAB is formed at these locations on the heterogeneous Ag substrate during pATP → DMAB. At positions 6, 13, 14, 15, 16, 18, and 19, Raman band appearing at ≈ 1365 cm^{-1} is assigned to the C-H bending mode resulting from the local structural deformation of DMAB molecules on the sample as reported previously by Uetsuki *et al.* (*J.*

Phys. Chem. C **2010,** *114,* 7515–7520). This indicates that the DMAB molecules are oriented differently at various locations on the heterogeneous Ag substrate.

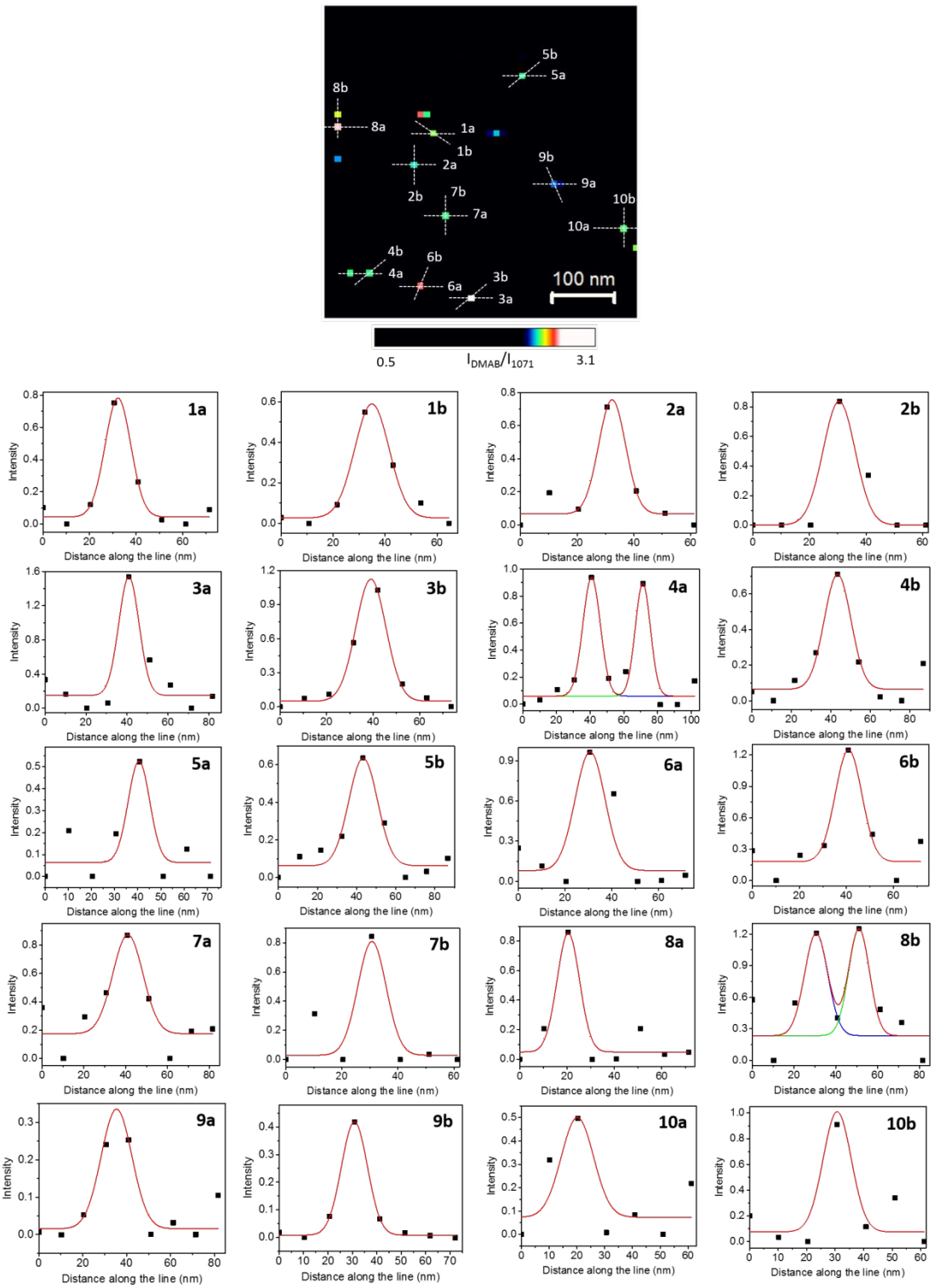

Figure S16. Line Profile analysis of the reaction hotspots in the pATP → DMAB TERS map. Top: TERS map of pATP → DMAB in aqueous environment shown in Figure 4d. Bottom: Intensity profiles along the lines marked as 1 – 10 in the TERS map on top in horizontal (a) and oblique (b) directions fitted with Gaussian curves with an average FWHM

of 13.5 ± 2.1 nm. This shows the highly localised nature of the reaction hotspots on the Ag substrate as well the nanoscale spatial resolution of TERS for mapping of these hotspots in an aqueous environment. The intensity scale on the *y*-axis represents the I_{DMAB}/I_{1071} ratio after baseline subtraction. See Table S2 for details.

Table S2. Spatial analysis of the reaction hotspots of pATP → DMAB TERS map using FWHM of the Gaussian fit to the line profiles in horizontal and oblique directions from 10 different locations shown in Figure S16.

Line profile	FWHM (nm)	
	Horizontal direction (a)	Oblique direction (b)
1	13.0	15.6
2	11.2	13.3
3	11.7	15.3
4	11.4	15.9
5	11.0	17.2
6	15.0	13.3
7	17.0	11.9
8	11.2	12.4
9	16.5	12.6
10	13.7	11.2
Average	**13.5 ± 2.1**	

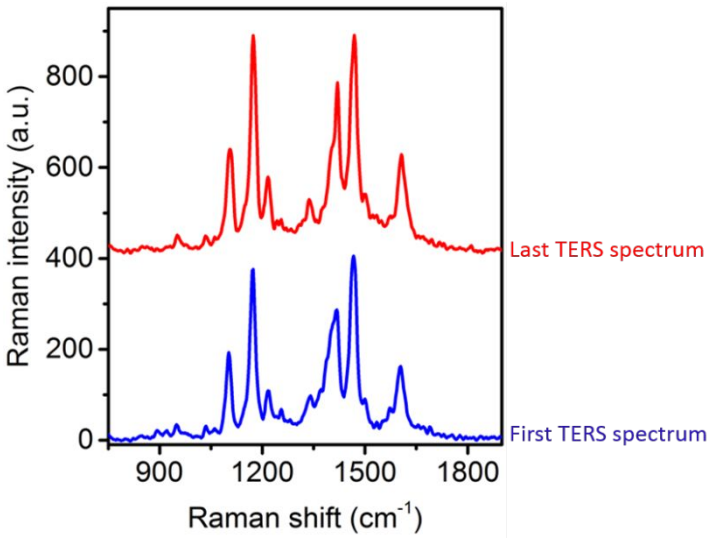

Figure S17. The first and the last spectrum measured in the TERS map is shown in Figure 4b. A similar signal intensity is observed in these TERS spectra shows the stability of ZrO_2-protected probe during the course of TERS mapping.